

In Silico Design of Monomolecular Drug Carriers for the Tyrosine Kinase Inhibitor Drug Imatinib Based on Calix- and Thiocalix[n]arene Host Molecules: A DFT and Molecular Dynamics Study

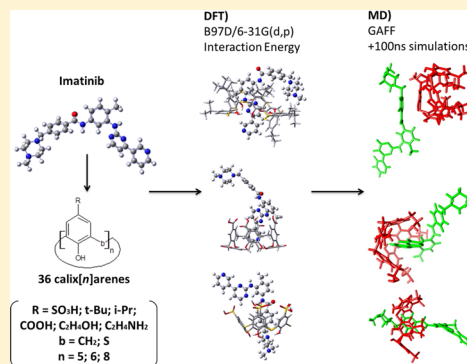
Rodrigo Galindo-Murillo,[†] María Eugenia Sandoval-Salinas,[‡] and Joaquín Barroso-Flores^{*,‡}

[†]Department of Medicinal Chemistry, College of Pharmacy, University of Utah, 2000 East 30 South Skaggs 201, Salt Lake City, Utah 84112, United States

[‡]Centro Conjunto de Investigación en Química Sustentable UAEM-UNAM, Carretera Toluca-Atlacomulco Km 14.5, Unidad San Cayetano, Toluca, Estado de México, C. P. 50200

S Supporting Information

ABSTRACT: The use of functionalized calix- and thia-calix[n]arenes is proposed as the basis for our *in silico* design of a suitable drug carrier for the tyrosine kinase inhibitor, Imatinib. Their mutual electronic properties and interaction energies, E_{int} , were assessed with the use of Density Functional Theory (DFT) methods under the NBODel methodology. Three structural variables for the host molecules were considered: R = {SO₃H (1), t-Bu (2), i-Pr (3), COOH (4), (CH₂)₂OH (5), (CH₂)₂NH₂ (6)}; b = {CH₂, S}; n = {5, 6, 8}, and two possible orientations for the insertion of Imatinib within the macrocycle cavity: pyridine moiety pointing inward (N1) and piperazine pointing inward (N2). In total, we explored 72 different assemblies. Initial molecular mechanics geometry optimizations with the UFF potential were undertaken for every host–guest complex, with further optimization at the B97D/6-31G(d,p) level of theory. Using the same optimized structures, Molecular Dynamics (MD) simulations were carried out on all 72 assemblies using the General Amber Force Field and the AMBER 12 MD package. Electronic parameters were fitted using the RESP method, and the complexes were run for 100 ns. Potential of mean force was obtained for the most stable systems using umbrella sampling and the Weighted Histogram Analysis Method. Calix[n]arenes families 1 and 5 (R = SO₃H and (CH₂)₂OH, respectively) with n = 6 constitute the most promising candidates to become drug carriers within our parameter space due to their more negative E_{int} values and increased flexibility to allow the inclusion of the drug.



INTRODUCTION

Imatinib (commercialized as Gleevec by Novartis) is a tyrosine kinase III inhibitor¹ which has become a successful chemotherapy agent in the treatment of patients with chronic myeloid leukemia (CML)² as well as with gastrointestinal stromal tumors (GIST);³ its chemical structure is shown in Figure 1. Although it is highly soluble and exhibits a bioavailability close to 98%,⁴ over 95% of serum Imatinib is bound to plasma

proteins such as albumin and α 1-acid glycoprotein,⁵ and only the portion left unbound is biologically active.⁶ Hence, a decrease in the concentration of free Imatinib has a potentially positive effect in increasing the efficiency of the drug, as well as decreasing the adverse side effects, such as skin rash, edema, and cardio toxicity, associated with its bioaccumulation in healthy tissues.⁷

According to Chapuy et al.,⁸ patients under treatment with Imatinib may develop an intrinsic resistance to the drug since the different kinds of intracellular ATP-bound cassette (namely ABCB1 and ABCG2) transporters expressed in progenitor leukemia cells facilitate lysosomal sequestration. It has also been found that a subtherapeutic Imatinib plasma level might be correlated to the mechanism of early drug resistance.⁹ In the case of GIST, more than half the number of patients treated with Imatinib show or develop different levels of resistance,¹⁰ which leads to the usage of additional simultaneous treatments. Additionally, genetic mutations affecting the expression of the

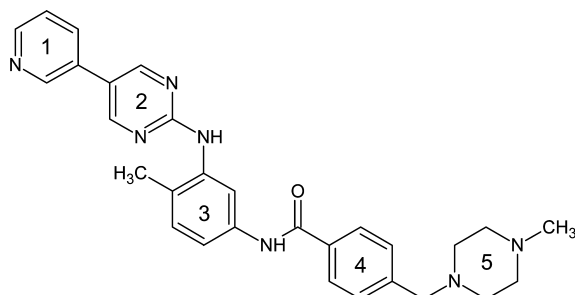


Figure 1. Chemical structure for Imatinib and ring numbering scheme.

transport system have been observed to correlate with lowered drug efficiency in a phenomenon called acquired pharmacokinetic drug resistance.^{10–12} The usage of a drug carrier might then decrease the probability of sequestration by the progenitor cells, which in turn would decrease the rate with which the resistance is developed. Extensive pharmacokinetic studies on Imatinib and other related drugs can be consulted elsewhere.¹³

Herein, we explore the electronic and energetic properties of calixarenes and thia-calixarenes and their inclusion complexes with Imatinib as a first step in proposing their use as candidates in the design of a suitable Imatinib carrier which may contribute to the enhancement of the drug's activity and a decrease of side effects associated with its bioaccumulation. Calix[*n*]arenes are a family of cone shaped macrocycles that are most commonly synthesized from the condensation of phenol with formaldehyde,¹⁴ which in recent times have known a growing interest as far as their molecular recognition capacities are concerned.^{15,16} These macrocycles possess a hydrophobic cavity that makes them a versatile kind of host molecule,¹⁷ since, as opposed to other macrocycles, they can be broadly functionalized, with which one may tune the affinity of the cavity, making them more selective toward various species, and at the same time the pendent functional groups provide binding sites for the guest molecules. Several conformations are available for these macrocycles, which increases as the number of *n* increases, the cone conformation being the most stable according to quantum mechanical calculations, molecular dynamics simulations, and experimental evidence.^{18,19} At their cone conformation, calixarenes possess a narrow rim, which is commonly referred to as lower rim, typically bearing hydroxyl groups from phenol. Because of their location at the narrow end of the cone, these hydroxyl groups are close enough to each other as to form a homodromic hydrogen bond system. On the other end, the so-called upper rim, calixarenes can bear almost any kind of functional groups; being wider, this end is readily available for accepting guest species inside the cavity of the macrocycle. Different kinds of calixarenes have also been used successfully in a broad spectrum of applications such as electrochemical or fluorescent sensors,^{20,21} protein recognition agents,²² and as molecular carriers extracting ionic species to nonpolar solvents, thus improving the solubility of nonpolar species into aqueous or other solutions with high permittivity.^{23,24}

The general structure of a calix[*n*]arene molecule is described in Figure 2, in which the three parameters used in this study are explicitly described, namely the bridge *b*, the upper rim functional groups R, and the cavity size *n*.

According to recent literature, calix[*n*]arenes show little to null toxicity,^{25–27} which is the first requirement to be complied to by any suitable drug carrier or drug delivery agent together with chemical stability and both improved pharmacokinetics and controlled release kinetics of its pharmaceutical pay-

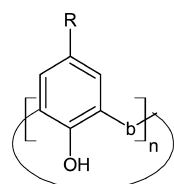


Figure 2. Chemical structure for the calix[*n*]arene family of compounds.

load.^{28,29} Previous successful efforts to generate a specific delivery agent for Imatinib have been published.³⁰ The use of polymolecular carriers for vascular drug delivery is widespread,³¹ but their biggest caveat is that while they increase circulation there is little penetration due to a wrong size fitting through the tumor's vessels.³² Since tumors tend to present a tortuous and poorly differentiated vasculature, they tend to be leaky, allowing for long-circulating agents to accumulate over time as a consequence of the so-called enhanced permeability and retention (EPR) effect, whose exploitation is considered a most effective strategy in "passive drug targeting." Most chemotherapy agents are rapidly cleared from systemic circulation by virtue of their low molecular weight reducing thus the effective concentration in the target tissue. After leaving the tumor blood vessels (extravasation), drug carriers need to penetrate into and distribute across the tissue in order to interact with as many cancer cells as possible and deliver the drug molecules. Polymolecular drug carriers such as dendrimers and liposomes have large sizes in comparison to the low molecular-weight drugs usually employed in chemotherapy; this reduces their penetration into more than one or two cell layers.^{33,34} Although Ehrlich's magic bullet concept, as originally conceived more than a century ago,³⁵ is at present time difficult to achieve, the usage of a carrier which modifies the pharmacokinetics of a drug could yield great therapeutic benefits by preventing its accumulation in nontargeted organs in its pharmaceutically active form.

It is, thus, of great interest to design a novel calixarene-based drug carrier specifically constructed to transport Imatinib. In this work, we study 36 different calix[*n*]arenes systems and their interaction energy with Imatinib using Quantum Mechanics (QM) and Molecular Dynamics (MD). We also study the free energy profiles using the Potential of Mean Force (PMF) of the calixarene–Imatinib complex formation.

METHODS

Quantum Mechanics Study. All calculations were carried out using the Gaussian 09, revision B.01 suite of programs.³⁶ Host–guest complexes were formed by manually docking the guest through either the pyridine (*N1*) or the piperazine (*N2*) ring inside the host cavities at the same height as the aromatic moieties of the calixarenes (see Figure 3). In both cases, we are considering the insertion of the drug from the upper rim and not from the lower rim since the former offers less steric hindrance. This procedure yields a total of 72 possible

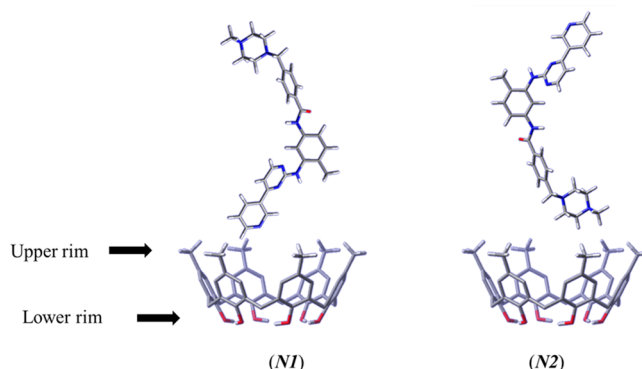


Figure 3. Orientations for the insertion of Imatinib within the macrocyclic cavities. Depiction of the macrocycle is not to scale with respect to the guest.

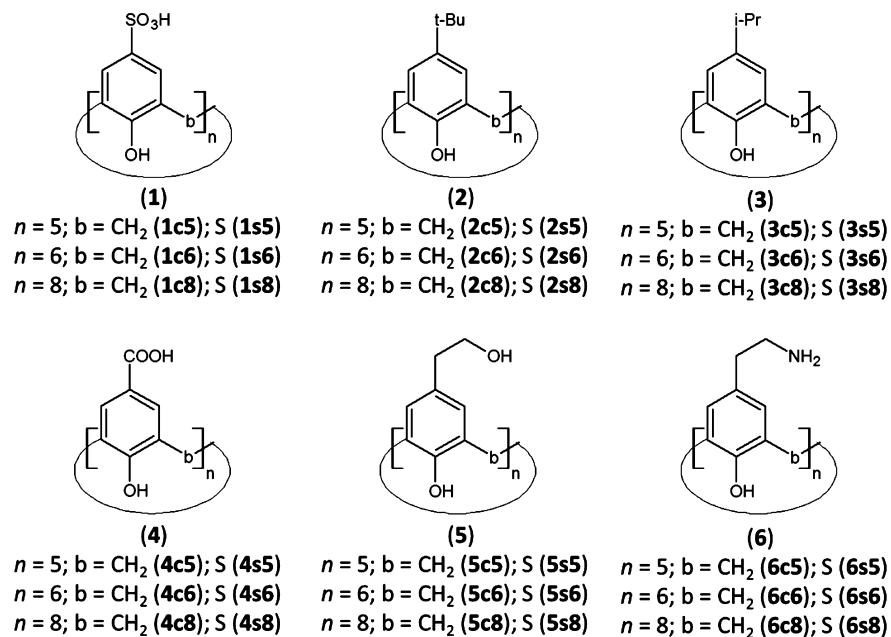


Figure 4. Naming scheme for the calix and thiocalix[*n*]arenes hosts under study. The first number indicates the functional group, whereas the last one indicates the size of the ring. The letter in between them, c or s, refers to the bridge considered, methylene or sulfide, respectively.

complexes from the 36 free hosts. The suffix @Ni is added to the naming scheme of the free host in order to distinguish the conformation in which the drug is introduced into its cavity. The resulting structures for all complexes were optimized at the Molecular Mechanics level using the UFF potential³⁷ as defined within Gaussian, in order to prevent anomalous contacts between fragments. The complexes were then further optimized at the B97D/6-31G(*d,p*) level, and the interaction energy, *E*_{int}, was assessed through the NBO deletion method (NBODel), as implemented in the NBO3.1 program,³⁸ which consists of calculating the energy change after deleting all elements in the Fock matrix mutual to the atoms of both fragments and rediagonalizing the resulting matrix.³⁹ The selected functional, B97-D, is a density functional of the generalized gradient approximation (GGA) type with adequate performance in describing noncovalently bound systems, dispersion effects, and long-range interactions.⁴⁰ We tested several hybrid type functionals to increase our accuracy, but B97-D provided the most reasonable convergence time. For clarity, interaction energy values are reported with a negative magnitude as to be comparable with the values obtained with Molecular Dynamics (MD) and Potential of Mean Force (PMF) values. Vibrational frequencies were calculated at the same level of theory for the optimized complexes in order to verify that the stationary points found are local minima on the potential energy surface. No imaginary frequencies were observed for any of the compounds under study.

Molecular Dynamics Study. Using the optimized geometries of the hosts and the guest molecules from the QM step, we applied a restrained electrostatic potential⁴¹ charge fit using the R.E.D. server (using the Gaussian 2009 C.01 interface, HF/6-31G*, 2-stage RESP fit qwt = 0.0005/0.001, compatible with the AMBER force fields).⁴² Force field parameters (bonded and nonbonded) were determined using the ANTECHAMBER and PARMCHK tools available from AMBER12 based on the General Amber Force Field (GAFF³⁶). The guest–host complex (*N*1 and *N*2 insertion modes) was then solvated using the TIP3P⁴⁴ water model in a periodic truncated

octahedron cell with a minimum water shell of 30.0 Å around the complex to ensure that the system will not interact with its periodic image. All 72 systems were explicitly solvated, minimized, heated, and equilibrated using the same procedure: (a) 1000 steps of steepest descent minimization followed by 1000 steps of conjugate gradients minimization applying a position restraint constant of 25 kcal/mol·Å² to the Imatinib–calixarene complex, (b) heating of the system in 5000 steps using the Langevin thermostat from 10 to 300 K using the same position restraint constant in the solute, (c) equilibration at 300 K in constant pressure was performed using a series of 25 000 step runs gradually lowering the value of the restraint constant until a value of 0.5 kcal/mol·Å². A total of 100 ns production simulation time with explicit solvation was performed using the CUDA version of the PMEMD Molecular Dynamics engine available in AMBER12.⁴⁵ The SHAKE⁴⁶ algorithm was applied to all hydrogen bonds, and a 2 fs time step was used for the heating, equilibration, and production simulations and a cutoff of 9 Å. Long range interactions were treated using the particle mesh EWALD,⁴⁷ and trajectory information was recorded every 500 steps. The MM-PBSA^{48,49} methodology was used to evaluate the relative interaction energies for all the systems using an ionic strength of 150 mM and implicit solvation constants of ϵ = 1.0 for dielectric solute and ϵ = 80 for the solvent. For all the simulations and to lower the computational time required, only the final 10 ns of the production MD runs were used for the energy analysis using 200 ps intervals. It has been shown that the MM-PBSA method yields more accurate results than the Generalized Born model (MM-GBSA⁴²). The Potential of Mean Force (PMF)^{50,51} was obtained using 15 distance restrained umbrella windows with a force constant of 1.2 kcal/mol·Å². For all the calixarenes, the anchor used for the Umbrella Sampling was calculated using all the oxygen atoms of the hydroxyl group of the phenol molecule (lower rim). This creates a center of mass in the center of the ring and allows proper docking of the guest molecule, without constraining the normal fluctuations of the hydroxyl group of each phenol molecule. The anchor for the guest molecule was located in the

nitrogen atoms of the pyrimidine ring for *N*1 simulations (ring 2) and carbon atoms C4, C5, and C6 of the phenyl ring (ring 4) for the *N*2 simulations. A distance restraint was applied using the anchor points between the host and the guest from 1 to 15 Å in 1 Å intervals for a total of 15 umbrella windows. Additional anchor atoms for the *N*1 orientation were located in ring 1 (pyridine ring) and nitrogen atoms of piperazine (ring 5) for *N*2, but these anchors allowed the guest molecule to move out of position outside the host molecule and also rotating toward the host molecule and forming interactions that interfered with the sampling. This fluctuation did not allow a proper docking inside the host molecule. The windows were explicitly solvated using the TIP3P water model, heated and equilibrated using the same procedure as the unrestrained MD simulations described above. Each window was run for a total of 1 ns individually. To increase the statistics of the PMF values, for each individual window of each system we ran a total of four simulations with randomized water positions in each case, and the PMF values were averaged. All umbrella sampling distributions were unbiased using Grossfield implementation⁵³ of the WHAM method.^{54,55} A PMF profile was obtained only for the lead systems (*vide infra*).

RESULTS AND DISCUSSION

The full space of structural parameters covered in the present study is depicted in Figure 4. Eighteen different calix[*n*]arenes and their corresponding 18 thiocalix[*n*]arene counterparts were studied for a total of 36 potential drug carriers. Initial structures for the free hosts are shown in Figures 5, 6, and 7 for *n* = 5, 6, and 8, respectively.

Table 1 collects all values of interaction energy between host and guest calculated at the B97D/6-31G(*d,p*) level of theory for

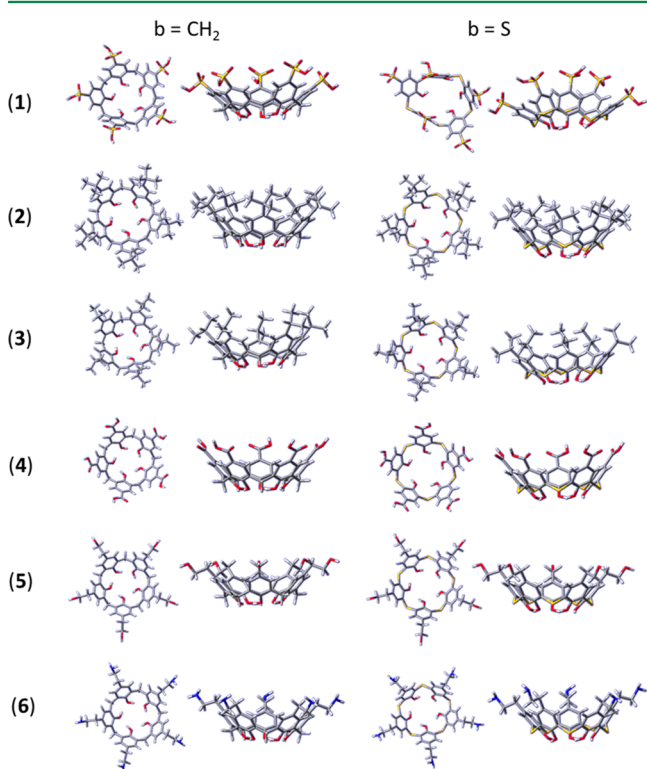


Figure 5. Free calix- and thiocalix[5]arenes hosts. Top and side views are shown.

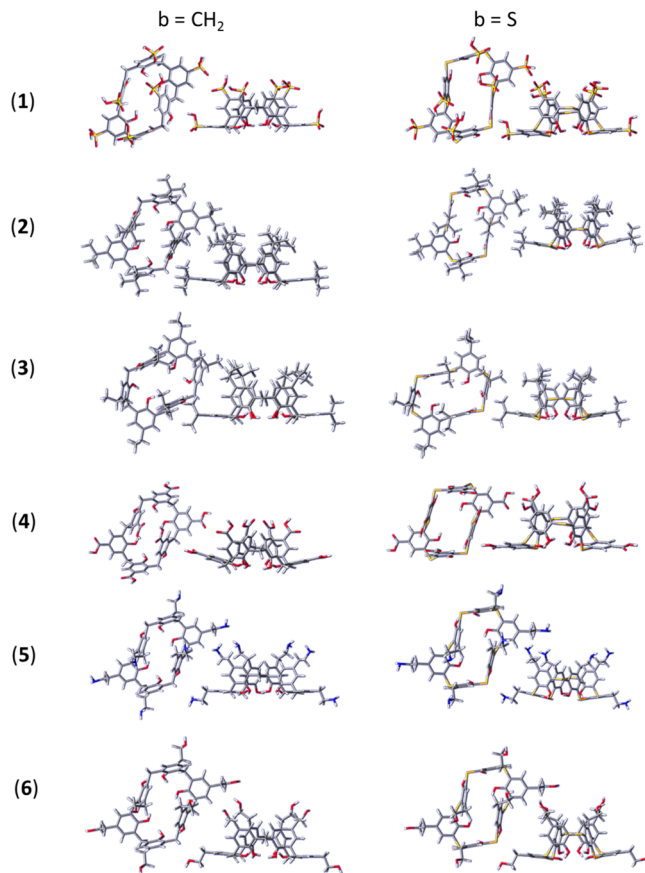


Figure 6. Free calix- and thiocalix[6]arenes hosts. Top and side views are shown.

all 72 complexes at their optimized geometries obtained at the same level of theory. From these results, we establish an arbitrary -138.36 kcal/mol (-6.0 eV) threshold, below which, we consider a stable host–guest interaction, which could be further preserved in solution, and thus, the corresponding macrocycles constitute our leads in the search for a suitable Imatinib carrier. This threshold value permits us to screen only the top third of the host guest complexes under study in order to focus only on the most stable inclusion complexes within our considered chemical space.

Thus, lead complexes with $E_{\text{int}} \leq -138.36$ kcal/mol (-6.0 eV) are (1c6)@N1, (5c6)@N1, (5c8)@N1, (1s5)@N1, (1s6)@N1, (5s6)@N1, (1s8)@N1, (4s8)@N1, (5s8)@N1, (1c5)@N2, (4c5)@N2, (1c6)@N2, (2c6)@N2, (4c6)@N2, (6c6)@N2, (1s5)@N2, (2s6)@N2, (4s6)@N2, (5s6)@N2, and (6s6)@N2. Figure 8 collects their optimized structures. From these 20 compounds, 15 exhibit an interaction energy value below an even tighter threshold of $E_{\text{int}} = -250.0$ kcal/mol. Our ideal drug carrier should be a stable compound, so its formation is chemically feasible yet not entirely stable kinetically in solution as to never release the drug into the affected tissue. The least suitable complexes within our study, arbitrarily similarly defined as those with $E_{\text{int}} \geq -69.18$ kcal/mol (-3.0 eV), are (1c5)@N1, (2c5)@N1, (3c5)@N1, (4c5)@N1, (5c5)@N1, (6c5)@N1, (2s5)@N1, (3s5)@N1, (4s5)@N1, (5s5)@N1, (2s6)@N1, (3s6)@N1, (2c5)@N2, (3c5)@N2, (6c5)@N2, (2s5)@N2, (3s5)@N2, (4s5)@N2, and (3s8)@N2. This procedure divides our chemical space in three sections which can be labeled as stable ($E_{\text{int}} \leq -138.36$ kcal/mol), labile ($E_{\text{int}} \geq -69.18$ kcal/mol), and intermediate (-138.36 kcal/mol $< E_{\text{int}}$

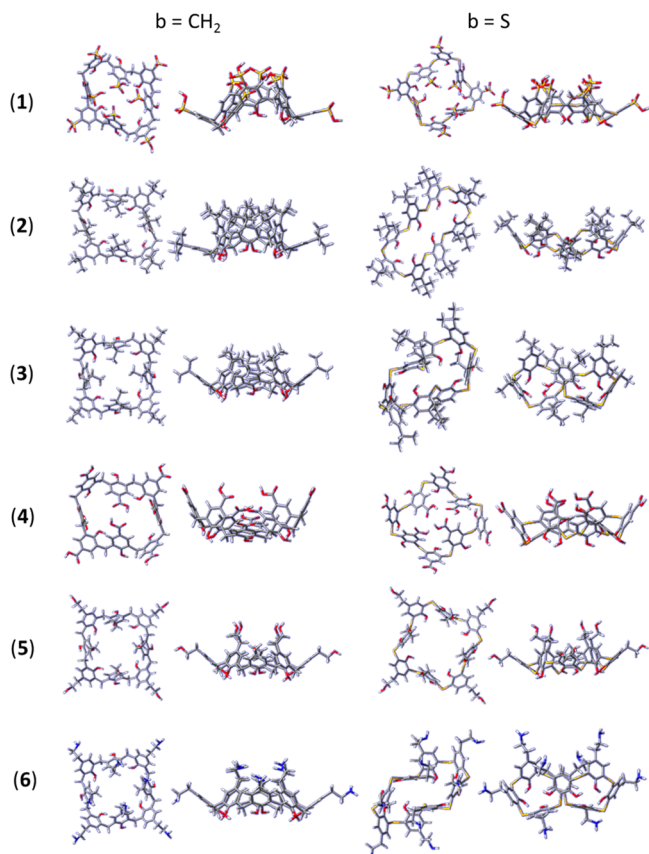


Figure 7. Free calix- and thiocalix[8]arenes hosts. Top and side views are shown.

< -69.18 kcal/mol). The first one is comprised of 20 compounds, and the latter of 19; the remaining 33 compounds comprise the intermediate section.

Molecular dynamics simulations yielded a high number of conformations of the Imatinib interacting with the calixarene macrocycle, which could be summarized in three different categories: (A) inclusion, in which the Imatinib molecule remains inside the calixarene for the entire simulation time in a rotaxane-like configuration; (B) partial inclusion, in which the Imatinib molecule is not crossing the calixarene ring but is forming specific nonbonding interactions with it; and (C) in which the Imatinib molecule has completely detached from the calixarene molecule, although it remains still close to the macrocycle. An example of these three conformations can be seen in Figure 9.

It must be noticed that a complete detachment and full solvation of the Imatinib molecule from the calixarene host was not observed in any of the 72 simulations. An average structure using the last 10 ns of the 100 ns simulation for all the systems is available in the Supporting Information. The A conformation is present in 51% of the simulations, B 32%, and C the remaining 16%. The N1 distribution is 17% A, 53% B, and 30% C, and the N2 is 84%, 11%, and 5%, respectively.

The A mode of interaction in which the Imatinib molecule remains inside the calixarene ring was mainly observed for the N2 insertion mode. This is expected since the N-methyl-piperazine moiety of Imatinib (N2) produces more steric clashes with the host molecule than a completely planar molecule. Also, this configuration shows a stable interaction mode between the Imatinib molecule and the calixarene early in the simulations as seen in the root-mean-square deviation (RMSd, refer to Supporting Information) and remains for the duration of the run. This stability is mainly because of two properties of the orientation of the system: the fact that the piperazine ring forms hydrogen bonds with the hydroxyl groups in the rim of the calixarene and the fourth ring of the Imatinib structure (see Figure 1) forms stacking interactions with the aromatic rings present in the calixarene ring (refer, for example, to structures (6s6)@N2, (4s6)@N2, (3s5)@N2, (6s5)@N2, and (4s5)@N2 in the Supporting Information). The B mode of interaction is observed when the Imatinib molecule moves toward the solvent in the upper rim of the calixarene ring and forms stacking interactions with the calixarene with either ring 1 or 2 from the ligand. This process takes from 10 to 20 ns, and once the Imatinib molecule forms the stacking, it remains there for the rest of the simulation. Examples of systems with the B type interaction are (1c5)@N1, (2c5)@N1, (3c5)@N1, (4c5)@N1, (5c5)@N1, (6c6)@N1, (2c6)@N1, (4c6)@N1, (5c6)@N1, (6c6)@N1, and (1c8)@N1; for a full listing, see Table 2. One interesting case is (2c8)@N2 in which the Imatinib started with the N-methyl-piperazine ring inside the calix[8]arene cavity, and during the simulation, the ligand moved outside the ring toward the solvent and turned 180° until the pyridine ring formed π-π stacking interactions with the eight-member ring. This process took 43 ns and remained in that particular configuration for the remainder of the run. The last form of interaction we found from the molecular dynamics simulations is called the C type, where the Imatinib leaves the calixarene host from the upper rim and binds to it from the other side of the molecule (outside the macrocycle). The ligand explores the calixarene through the simulation until it forms a stacking interaction with any of the phenol rings and remains there for the length of the simulation, for example, in (2s6)@N2, (3c6)@N1, and (3s6)@N1. This process takes an average of 20 ns

Table 1. Energy Change (kcal/mol) after Deletion of Mutual Elements to Host and Guest in the Fock Matrix Calculated at the B97D/6-31G(*d,p*) Level of Theory for the Various Complex Structures under Study

	N1 (pyridine)						N2 (piperazine)					
	CH ₂			S			CH ₂			S		
	5	6	8	5	6	8	5	6	8	5	6	8
(1) SO ₃ H	-62.8	-261.6	-88.5	-165.5	-142.9	-274.1	-271.6	-280.6	-137.0	-350.4	-130.9	-104.7
(2) <i>t</i> -Bu	-50.0	-78.7	-89.4	-47.6	-59.0	-91.9	-45.2	-289.3	-116.8	-49.6	-288.6	-103.9
(3) <i>i</i> -Pro	-46.7	-101.9	-97.0	-44.4	-53.8	-87.7	-42.2	-100.1	-77.7	-46.1	-95.8	-69.0
(4) COOH	-47.4	-112.6	-122.3	-52.4	-106.3	-150.7	-278.7	-288.3	-115.1	-64.1	-268.6	-82.0
(5) (CH ₃) ₂ OH	-46.0	-264.2	-143.1	-46.3	-271.8	-161.9	-79.5	-127.3	-88.8	-90.6	-279.9	-131.6
(6) (CH ₃) ₂ NH ₂	-61.3	-138.2	-103.4	-83.0	-126.2	-78.3	-54.0	-291.2	-116.5	-73.1	-282.3	-98.3

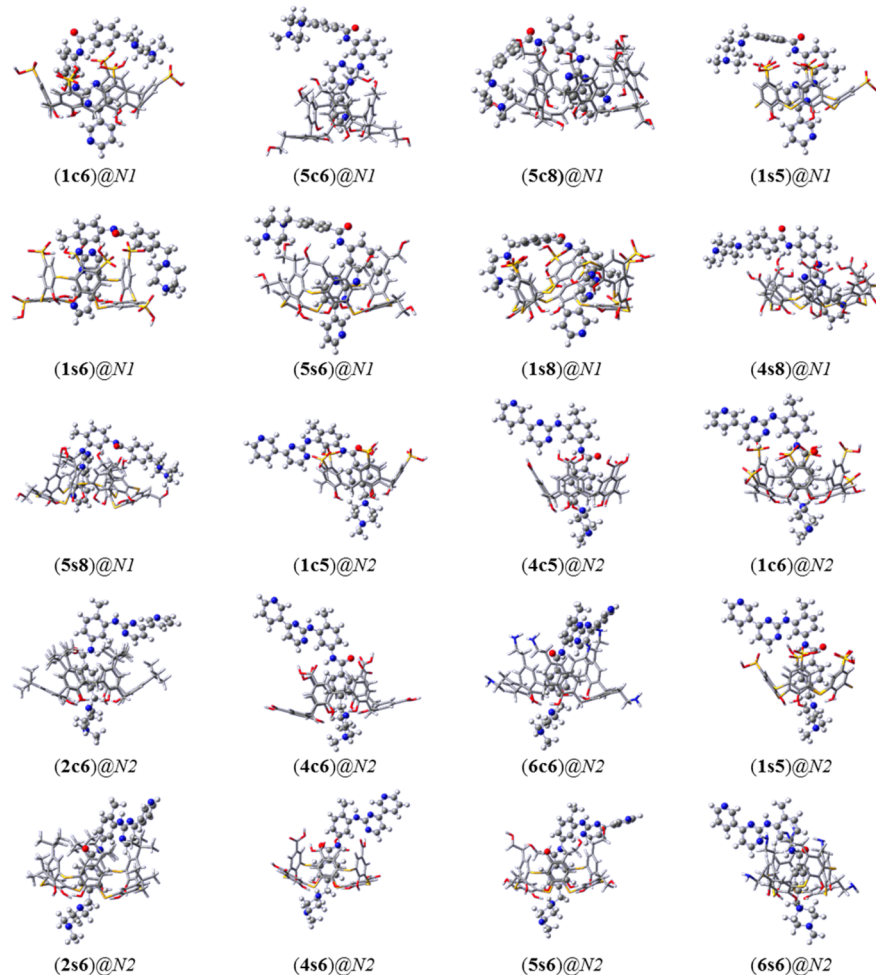


Figure 8. Optimized structure for lead compounds with $E_{\text{int}} \leq -138.36$ kcal/mol. Optimizations carried at the B97D/6-31G(d,p) level of theory.

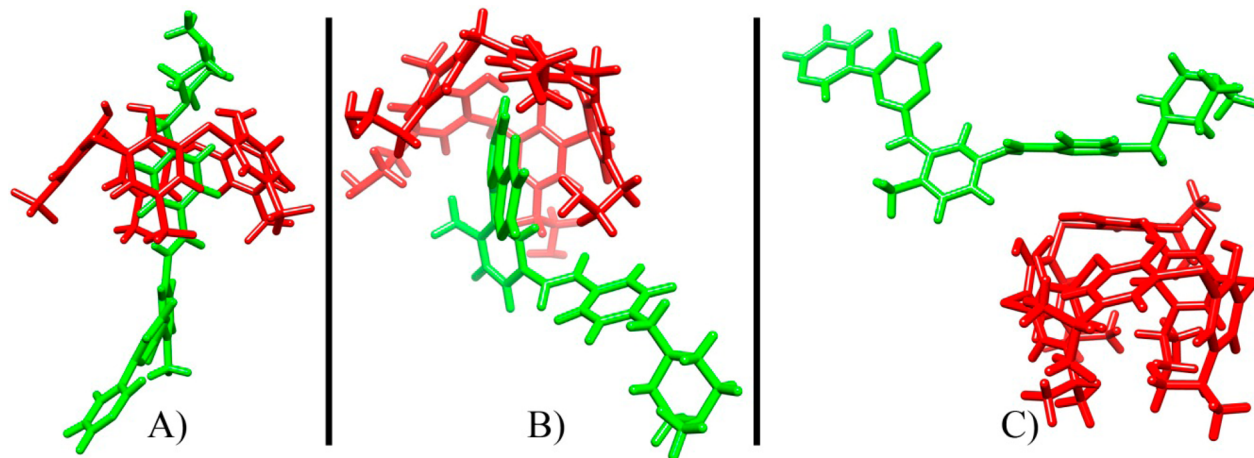


Figure 9. Three of the observed conformations for the 72 100 ns MD simulations (calixarene in red and Imatinib in green). (A) The ligand is inside the calix-arene ring (1s5)@N2. (B) The ligand is interacting with the inner part of the calix-arene, but not crossing it (6c5)@N1, and (C) the ligand is interacting with the calix-arene outside the ring (3s6)@N1.

on all of the conformation in which this interaction was observed.

One of the main goals of this work is to determine the energetic behavior that these complexes present in order to give some insight for the experimental synthesis and avoid wasting resources and time developing drug carriers that will be either too strong to let the drug detach or too mild so that it will not

carry the drug at all. $\Delta G_{\text{binding}}$ values for all 72 different simulations are summarized in Table 3. The complexes have a range of binding energies from -24 to -3 kcal/mol. It is expected that as the size of the system increases, the binding energy required to maintain the complex together will also increase. Overall, calix[5]arenes show values of $\Delta G_{\text{binding}}$ 4–5 kcal/mol higher than calix[6]arenes, and these in turn show an

Table 2. Modes of Interaction for 100 ns of Molecular Dynamics Simulation^a

	N1 (pyridine)						N2 (piperazine)					
	CH ₂			S			CH ₂			S		
	5	6	8	5	6	8	5	6	8	5	6	8
1-SO ₃ H	B	A	B	B	A	B	A	A	A	A	A	A
2-t-Bu	B	B	B	C	C	B	A	A	B	A	C	A
3-i-Pr	B	C	A	C	C	C	A	A	B	A	A	B
4-COOH	B	B	A	B	C	C	A	A	A	A	A	A
5-(CH ₂) ₂ OH	B	B	B	C	A	C	A	A	B	A	A	A
6-(CH ₂) ₂ NH ₂	B	B	A	B	B	C	A	A	C	A	A	A

^a(A) Imatinib inside of the calix-arene ring. (B) Imatinib forming pi-pi stacking interactions. (C) External interaction outside the ring (refer to Figure 9).

Table 3. MM-PBSA Binding Energy Results in kcal/mol for the 72 MD Runs

	N1 (pyridine)						N2 (piperazine)					
	CH ₂			S			CH ₂			S		
	5	6	8	5	6	8	5	6	8	5	6	8
1-SO ₃ H	-9.7	-12.8	-15.7	-5.0	-3.0	-11.2	-13.2	-11.8	-18.4	-5.0	-11.2	-14.6
2-t-Bu	-17.1	-19.6	-24.4	-13.5	-15.0	-21.1	-7.7	-17.9	-21.7	-16.0	-20.4	-20.4
3-i-Pr	-15.1	-19.1	-21.6	-13.6	-14.7	-22.5	-11.2	-19.9	-16.7	-19.7	-22.5	-23.3
4-COOH	-16.9	-16.7	-20.3	-12.1	-14.6	-14.5	-5.9	-15.4	-22.8	-12.8	-16.0	-19.2
5-(CH ₂) ₂ OH	-14.2	-16.7	-16.7	-17.4	-18.9	-16.2	-5.7	-15.0	-21.6	-14.6	-18.4	-23.3
6-(CH ₂) ₂ NH ₂	-18.1	-20.9	-19.1	-19.0	-19.4	-22.9	-9.3	-17.5	-21.0	-14.6	-20.2	-21.0

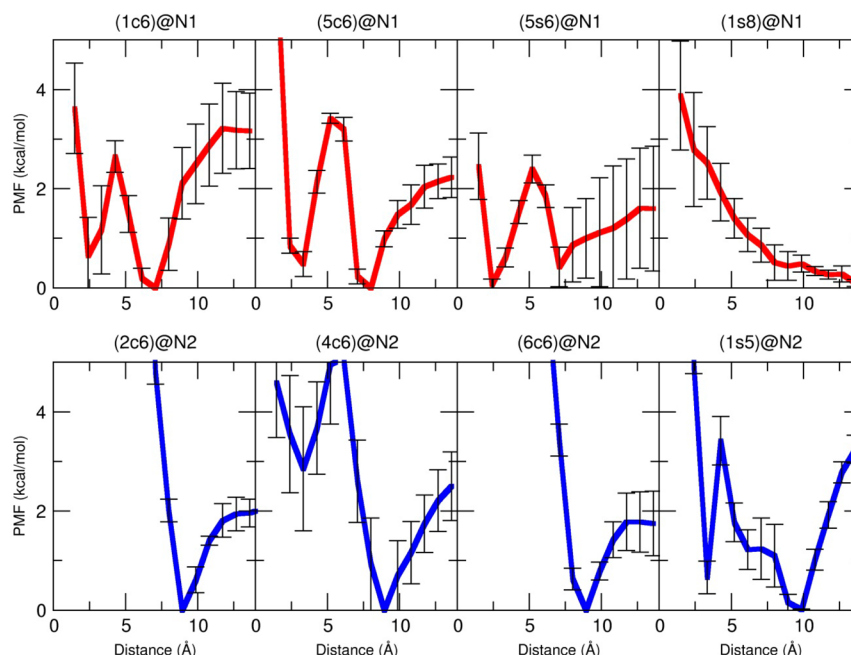


Figure 10. Potential of mean force profiles for the four most stable complexes for positions N1 and N2 from the QM simulations. Red, complexes in the N1 position; blue, N2 position.

average value of 5–6 kcal/mol higher than calix[8]arenes. The effect of the size of the calixarene is observed with the QM energy calculations, although to a lesser extent mainly due to the lack of energy involved in the reorganization of the solvent. The difference between the QM and the MD interaction energy values can be related to several effects. Using the MM-PBSA approach in the MD simulations, the binding free energy is obtained by the difference between the desolvation energy and the bound complex energy⁵⁶ and does not include any energetic values directly derived from bonded parameters

(bond length, angles and dihedrals) from either the host or the guest molecules, which translates to a loss of energy of 3–11 kcal/mol.^{57–59} QM simulations were run in the gas phase, which yields an energy difference between this and the corresponding solvated system of about 2–3 kcal/mol.^{60,61}

Systems with the R = t-Bu, R = i-Pr, and R = (CH₂)₂NH₂ substituents have the lowest binding energy of all the complexes (Table 3 and S1 Figures). The presence of these groups in the upper rim allows nonbonded interactions with the section of the Imatinib molecule that is not forming the

$\pi-\pi$ stacking with the cavity of the calixarene. *tert*-Butyl and *isopropyl* reorient toward ring 2 (for N1 orientation) and ring 3 (for the N2 orientation), forming a CH- π interaction. The *t*-Bu residue has an extra methyl group which increases the number of possible conformations. For R = COOH, R = (CH₂)₂OH, R = (CH₂)₂NH₂, and R = SO₃H, no interaction was found between the calixarene and the Imatinib, these residues remain solvated during the simulation.

The potential of mean force profile was calculated for the four most stable complexes of the QM analysis, for position N1 [(1c6)@N1, (5c6)@N1, (5s6)@N1, (1s8)@N1] and N2 [(2c6)@N2, (4c6)@N2, (6c6)@N2, (1s5)@N2], and is presented in Figure 10. The flexibility of the Imatinib molecule and the substituent present in the calixarenes allows for multiple interaction points, although in most cases, only one zero energy point interaction is found. In the N1 position, when ring 2 of Imatinib is used as the anchor point, a minimum PMF value is found for complexes (1c6)@N1 and (5c6)@N1 between 7 and 8 Å. Also, in these simulations we first found a stable point at a distance of 2.8 Å, which corresponds to the ring 2 parallel to the aromatic rings that make the cavity. As distance is increased, ring 1 of Imatinib reorients to the walls of the host molecule to form the stable complex. After this, increasing the distance results in multiple arrangements with the substituents of the host molecule and rings 3 and 4 of Imatinib. In the case of (5s6)@N1, the most stable configuration is with the ring 2 oriented to the aromatic groups of the cavity. Although it is also a six-member ring, the sulfur atom present in the host molecule forms a cavity configuration that allows a smaller volume, facilitating the formation of interactions with the aromatic moieties of both guest and host molecule. For (1s8)@N1, the large volume of the cavity formed by the eight member ring allows solvent molecules to enter the cavity, making any interaction with the guest molecule difficult. This of course was not seen by the gas phase QM calculations. Moreover, the group restraints do not allow the guest molecule to approach any of the walls of the cavity, fixing it to the axial center of the ring. It is clear that the calix[8]arene systems allow the guest to interact with an overall reduced energy profile as a result of the higher cavity volume caused by the eight-unit ring.

For the N2 position, all four complexes present a PMF minimum when the center of mass of the hydroxyl groups of the lower rim of the host molecule and the ring 5 from Imatinib are at a distance of ~9 Å. The values higher than 5 kcal/mol in the distance range between 0 and 6 Å correspond to the bulky N-methylpiperazine ring crossing the hydroxyl groups of the host molecule, causing multiple steric clashes between both molecules and decreasing the stability of the interaction. In the case of (1s5)@N2, ring 5 orients to the aromatic rings of the cavity at a distance of ~3 Å, stabilizing the interaction to a value of ~1 kcal/mol (Figure 10, bottom right); this is not the case with the other three six-membered ring complexes, because the cavity provides more space. Since the guest molecule is at the center of the cavity, the formation of stable interactions of the ring 4 of Imatinib with the walls of the cavity is less frequent. PMF analysis suggests the formation of $\pi-\pi$ stacking interactions as the preferred configuration. Although MD force fields are of an empirical nature, the AMBER force field used in this work has an acceptable description of the stacking interactions.^{62–64} The nature of the two interaction modes (N1 and N2) is similar in all the systems. The first three windows correspond to an unstable configuration with a high number of

steric clashes between guest and host molecules, which translate to a quick rearrangement mainly of the calixarene to a different conformation. Between windows 4 and 10, the guest molecule shifts positions until the stacking interaction is formed and also the rest of the Imatinib molecule forms a stable interaction with the substituents of the calixarene.

CONCLUSIONS

Twenty complexes which exhibit an interaction energy value below an arbitrarily chosen threshold $E_{\text{int}} \leq -6.0$ eV, as obtained from DFT/NBODEl computations at the B97D/6-31G(*d,p*) level of theory, were selected as lead candidates in the search for a suitable carrier for Imatinib. These are thought to form the most stable complexes *in vacuo* and were used as a starting point of our MD simulations in order to assess the drug release over time. MD simulations allowed studying the different interactions of the guest molecule with the host and the complete solvated system. Calix[6]arenes are the most suitable size of carriers for Imatinib in terms of cavity size according to the interaction energies calculated. The presence of H-bond donor functional groups on the upper rim, such as SO₃H in family 1 and (CH₂)₂OH in family 2, allows for further stabilization of the complex by binding to the N atoms on Imatinib. The presence of S-bridges (*b* = S) is seemingly slightly preferred energetically over CH₂ bridges (*b* = CH₂) by the guest, however in the latter case, host guest interaction energies tend to be higher. Insertion of Imatinib through the piperazine end, N2 mode, is the preferred conformation in the lead compounds, whereas the N1 mode was the predominant binding mode in compounds with $E_{\text{int}} \geq -3.0$ eV, although this value is mostly attributed to the presence of functional groups that interact poorly with Imatinib.

From Table 1, we can conclude that macrocycles with *n* = 5 tend to yield in general poor results concerning their inclusion of Imatinib, presumably due to higher steric hindrance, although the (1s5)@N2 compound exhibits the most stable value of E_{int} (~−350.4 kcal/mol). It is also noticeable from Table 1 that, in general, compound families 2 and 3 (*R* = *t*-Bu and iPr, respectively) are the least suitable functional groups to be used in the upper rim since their E_{int} values tend to be the lowest, whereas compound family 1 (*R* = SO₃H) seems the most promising by virtue of their higher exhibited E_{int} values, meaning that family 1 yields more stable inclusion complexes than families 2 or 3. Although most of the complexes found to be more stable are in the N2 interaction position, these conformations were either manually docked or restrained as in the MD simulations. Future efforts will be focused on running unbiased, unrestrained microsecond MD simulations to study the process of inclusion of the Imatinib-calixarene systems.

ASSOCIATED CONTENT

S Supporting Information

Average structures of the 72 MD simulations (using the last 10 ns), plots of the root-mean-square deviations of 100+ ns MD simulations of compounds on Table 3, initial geometries for all 36 free calix[n]arene hosts, and optimized geometries for all 72 inclusion complexes under study. This information is available free of charge via the Internet at <http://pubs.acs.org/>.

AUTHOR INFORMATION

Corresponding Author

*E-mail: jbarroso@unam.mx.

Notes

The authors declare no competing financial interest.

ACKNOWLEDGMENTS

J.B.-F. is thankful to UNAM for the financial support under project IA200111 as well as to DGTIC-UNAM for granting access to their supercomputing facilities known as *Kan Balam*. R.G.-M. is thankful to the Center for High Performance Computing of the University of Utah for computer time.

REFERENCES

- (1) Gschwind, H.-P.; Pfaar, U.; Waldmeier, F.; Zollinger, M.; Sayer, C.; Zbinden, P.; Hayes, M.; Pokorny, R.; Seiberling, M.; Ben-Am, M.; Peng, B.; Gross, G. *Drug Metab. Dispos.* **2005**, *33*, 1503–1512.
- (2) O'Brien, S. G.; Guilhot, F.; Larson, R. A.; Gathmann, I.; Baccarani, M.; Cervantes, F.; Cornelissen, J. J.; Fischer, T.; Hochhaus, A.; Hughes, T.; Lechner, K.; Nielsen, J. L.; Rousselot, P.; Reiffers, J.; Saglio, G.; Shepherd, J.; Simonsson, B.; Gratwohl, A.; Goldman, J. M.; Kantarjian, H.; Taylor, K.; Verhoef, G.; Bolton, A. E.; Capdeville, R.; Druker, B. *J. N. Engl. J. Med.* **2003**, *348*, 994–1004.
- (3) Ksienski, D. *Clin. Med. Insights: Oncol.* **2011**, *5*, 365–379.
- (4) Peng, B.; Hayes, M.; Resta, D.; Racine-Poon, A.; Druker, B. J.; Talpaz, M.; Sawyers, C. L.; Rosamilia, M.; Ford, J.; Lloyd, P.; Capdeville, R. *J. Clin. Oncol.* **2004**, *22*, 935–942.
- (5) Peng, B.; Dutreix, C.; Mehring, G.; Hayes, M. J.; Ben-Am, M.; Seiberling, M.; Pokorny, R.; Capdeville, R.; Lloyd, P. *J. Clin. Pharmacol.* **2004**, *44*, 158–162.
- (6) Peng, B.; Lloyd, P.; Schran, H. *Clin. Pharmacokinet.* **2005**, *44*, 879–894.
- (7) Kerkelä, R.; Grazette, L.; Yacobi, R.; Iliescu, C.; Patten, R.; Beahm, C.; Walters, B.; Shevtsov, S.; Pesant, S.; Clubb, F. J.; Rosenzweig, A.; Salomon, R. N.; Van Etten, R. A.; Alroy, J.; Durand, J.-B.; Force, T. *Nat. Med.* **2006**, *12*, 908–916.
- (8) Chapuy, B.; Panse, M.; Radunski, U.; Koch, R.; Wenzel, D.; Inagaki, N.; Haase, D.; Truemper, L.; Wulf, G. G. *Haematologica* **2009**, *94*, 1528–1536.
- (9) Demetri, G. D.; Wang, Y.; Wehrle, E.; Racine, A.; Nikolova, Z.; Blanke, C. D.; Joensuu, H.; von Mehren, M. *J. Clin. Oncol.* **2009**, *27*, 3141–3147.
- (10) Druker, B. *J. Blood* **2008**, *112*, 4808–4817.
- (11) Takahashi, N.; Miura, M.; Scott, S. A.; Kagaya, H.; Kameoka, Y.; Tagawa, H.; Saitoh, H.; Fujishima, N.; Yoshioka, T.; Hirokawa, M.; Sawada, K. *J. Hum. Genet.* **2010**, *55*, 731–737.
- (12) Eechoute, K.; Sparreboom, A.; Burger, H.; Franke, R. M.; Schiavon, G.; Verweij, J.; Loos, W. J.; Wiemer, E. A. C.; Mathijssen, R. H. *J. Clin. Cancer Res.* **2011**, *17*, 406–415.
- (13) Van Erp, N. P.; Gelderblom, H.; Guchelaar, H.-J. *Cancer Treat. Rev.* **2009**, *35*, 692–706.
- (14) Redshaw, C. *Coord. Chem. Rev.* **2003**, *244*, 45–70.
- (15) Mutihac, L.; Lee, J. H.; Kim, J. S.; Vicens, J. *Chem. Soc. Rev.* **2011**, *40*, 2777–2796.
- (16) Joseph, R.; Chinta, J. P.; Rao, C. P. *Inorg. Chim. Acta* **2010**, *363*, 2833–2839.
- (17) Barroso-Flores, J.; Silaghi-Dumitrescu, I.; Petrar, P. M.; Kunsági-Máté, S. *J. Incl. Phenom. Macrocycl. Chem.* **2012**, *75*, 39–46.
- (18) Hong, J.; Ham, S. *Tetrahedron Lett.* **2008**, *49*, 2393–2396.
- (19) Mokhtari, B.; Pourabdollah, K. *Can. J. Chem.* **2012**, *90*, 560–566.
- (20) Kim, J. S.; Quang, D. T. *Chem. Rev.* **2007**, *107*, 3780–3799.
- (21) El Nashar, R. M.; Wagdy, H. A. A.; Aboul-Enein, H. Y. *Curr. Anal. Chem.* **2009**, *5*, 249–270.
- (22) Coleman, A. W.; Perret, F.; Moussa, A.; Dupin, M.; Guo, Y.; Perron, H. *Top. Curr. Chem.* **2007**, *277*, 31–88.
- (23) Kunsági-Máté, S.; Vasapollo, G.; Szabó, K.; Bitter, I.; Mele, G.; Longo, L.; Kollár, L. *J. Incl. Phenom. Macrocycl. Chem.* **2007**, *60*, 71–78.
- (24) Kunsági-Máté, S.; Szabó, K.; Bitter, I.; Nagy, G.; Kollár, L. *Tetrahedron Lett.* **2004**, *45*, 1387–1390.
- (25) Perret, F.; Coleman, A. W. *Chem. Commun. (Camb.)* **2011**, *47*, 7303–7319.
- (26) Martin, A. D.; Houlihan, E.; Morellini, N.; Eggers, P. K.; James, E.; Stubbs, K. A.; Harvey, A. R.; Fitzgerald, M.; Raston, C. L.; Dunlop, S. A. *ChemPlusChem* **2012**, *77*, 308–313.
- (27) Oliveira, M. C.; de Reis, F. S.; de Fátima, Â.; Magalhães, T. F. F.; Silva, D. L.; da Porto, R. R.; Watanabe, G. A.; Martins, C. V. B.; Silva, D. L.; da Ruiz, A. L. T. G.; Fernandes, S. A.; de Carvalho, J. E.; de Resende-Stoianoff, M. A. *Lett. Drug Des. Discovery* **2012**, *9*, 30–36.
- (28) Huggins, D. J.; Sherman, W.; Tidor, B. *J. Med. Chem.* **2012**, *55*, 1424–1444.
- (29) Muro, S. *J. Controlled Release* **2012**, *164*, 125–137.
- (30) Dolman, M. E. M.; van Dorenmalen, K. M. A.; Pieters, E. H. E.; Lacombe, M.; Pato, J.; Storm, G.; Hennink, W. E.; Kok, R. J. *J. Controlled Release* **2012**, *157*, 461–468.
- (31) Koren, E.; Torchilin, V. P. *IUBMB Life* **2011**, *63*, 586–595.
- (32) Lammers, T.; Kiessling, F.; Hennink, W. E.; Storm, G. *J. Controlled Release* **2012**, *161*, 175–187.
- (33) Dreher, M. R.; Liu, W.; Michelich, C. R.; Dewhirst, M. W.; Yuan, F.; Chilkoti, A. *J. Natl. Cancer Inst.* **2006**, *98*, 335–44.
- (34) Popović, Z.; Liu, W.; Chauhan, V. P.; Lee, J.; Wong, C.; Greytak, A. B.; Insin, N.; Nocera, D. G.; Fukumura, D.; Jain, R. K.; Bawendi, M. G. *Angew. Chem., Int. Ed.* **2010**, *49*, 8649–8652.
- (35) Strebhardt, K.; Ullrich, A. *Nat. Rev. Cancer* **2008**, *8*, 473–480.
- (36) Frisch, M. J.; Trucks, G. W.; Schlegel, H. B.; Scuseria, G. E.; Robb, M. A.; Cheeseman, J. R.; Montgomery, J. A.; Vreven, T.; Kudin, K. N.; Burant, J. C.; Millam, J. M.; Iyengar, S. S.; Tomasi, J.; Barone, V.; Mennucci, B.; Cossi, M.; Scalmani, G.; Rega, N.; Petersson, G. A.; Nakatsuji, H.; Hada, M.; Ehara, M.; Toyota, K.; Fukuda, R.; Hasegawa, J.; Ishida, M.; Nakajima, T.; Honda, Y.; Kitao, O.; Nakai, H.; Klene, M.; Li, X.; Knox, J. E.; Hratchian, H. P.; Cross, J. B.; Bakken, V.; Adamo, C.; Jaramillo, J.; Gomperts, R.; Stratmann, R. E.; Yazyev, O.; Austin, A. J.; Cammi, R.; Pomelli, C.; Ochterski, J. W.; Ayala, P. Y.; Morokuma, K.; Voth, G. A.; Salvador, P.; Dannenberg, J. J.; Zakrzewski, V. G.; Dapprich, S.; Daniels, A. D.; Strain, M. C.; Farkas, O.; Malick, D. K.; Rabuck, A. D.; Raghavachari, K.; Foresman, J. B.; Ortiz, J. V.; Cui, Q.; Baboul, A. G.; Clifford, S.; Cioslowski, J.; Stefanov, B. B.; Liu, G.; Liashenko, A.; Piskorz, P.; Komaromi, I.; Martin, R. L.; Fox, D. J.; Keith, T.; Al-Laham, M. A.; Peng, C. Y.; Nanayakkara, A.; Challacombe, M.; Gill, P. M. W.; Johnson, B.; Chen, W.; Wong, M. W.; Gonzalez, C.; Pople, J. A. *Gaussian 09*, rev. B.01; Gaussian Inc.: Wallingford, CT, 2009.
- (37) Rappe, A. K.; Casewit, C. J.; Colwell, K. S.; Goddard, W. A.; Skiff, W. M. *J. Am. Chem. Soc.* **1992**, *114*, 10024–10035.
- (38) Glendening, E. D.; Reed, A. E.; Carpenter, J. E.; Weinhold, F. NBO: Theoretical Chemistry Institute, University of Wisconsin: Madison, WI, 2010.
- (39) Weinhold, F. In *Encyclopedia of Computational Chemistry*; Schleyer, P., Allinger, N. L., Clark, T., Gasteiger, J., Kollman, P. A., Schaefer, H. F., Schreiner, P. R., Eds.; John Wiley & Sons, Ltd., University of Wisconsin: Madison, WI, 2002; pp 1792–1811.
- (40) Grimme, S. *J. Comput. Chem.* **2006**, *27*, 1787–1799.
- (41) Bayly, C. I.; Cieplak, P.; Cornell, W. D.; Kollman, P. A. *J. Phys. Chem.* **1993**, *97*, 10269–10280.
- (42) Vanquelef, E.; Simon, S.; Marquant, G.; Garcia, E.; Klimerak, G.; Delepine, J. C.; Cieplak, P.; Dupradeau, F. *Nucleic Acids Res.* **2011**, *39*, W511–517.
- (43) Wang, J.; Wolf, R. M.; Caldwell, J. W.; Kollman, P. A.; Case, D. A. *J. Comput. Chem.* **2004**, *25*, 1157–1174.
- (44) Jorgensen, W. L.; Chandrasekhar, J.; Madura, J. D.; Impey, R. W.; Klein, M. L. *J. Chem. Phys.* **1983**, *79*, 926.
- (45) Case, D. A.; Cheatham, T. E. I.; Darden, T.; Gohlke, H.; Luo, R.; Merz, K. M.; Onufriev, A.; Simmerling, C.; Wang, B.; Woods, R. J. *J. Comput. Chem.* **2005**, *26*, 1668–1688.
- (46) Ryckaert, J.-P.; Ciccotti, G.; Berendsen, H. J. *J. Comput. Phys.* **1977**, *23*, 327–341.
- (47) Essmann, U.; Perera, L.; Berkowitz, M. L.; Darden, T.; Lee, H.; Pedersen, L. G. *J. Chem. Phys.* **1995**, *103*, 8577.

- (48) Srinivasan, J.; Cheatham, T. E. I.; Cieplak, P.; Kollman, P. A.; Case, D. A. *J. Am. Chem. Soc.* **1998**, *120*, 9401–9409.
- (49) Hansson, T.; Marelius, J.; Aqvist, J. *J. Comput.-Aided Mol. Des.* **1998**, *12*, 27–35.
- (50) Hou, T.; Wang, J.; Li, Y.; Wang, W. *J. Chem. Inf. Theory* **2010**, *51*, 69–82.
- (51) Straatsma, T. P.; McCammon, J. A. *Annu. Rev. Phys. Chem.* **1992**, *43*, 407–435.
- (52) Beveridge, D. L.; DiCapua, F. M. *Annu. Rev. Biophys. Biophys. Chem.* **1989**, *18*, 431–492.
- (53) Grossfield, A. WHAM: *The Weighted Histogram Analysis Method*. <http://membrane.urmc.rochester.edu/content/wham>.
- (54) Kumar, S.; Rosenberg, J. M.; Bouzida, D.; Swendsen, R. H.; Kollman, P. A. *J. Comput. Chem.* **1992**, *13*, 1011–1021.
- (55) Roux, B. *Comput. Phys. Commun.* **1995**, *91*, 275–282.
- (56) Wang, J.; Dixon, R.; Kollman, P. A. *Proteins* **1999**, *34*, 69–81.
- (57) Lazaridis, T.; Masunov, A.; Gandolfo, F. *Proteins* **2002**, *47*, 194–208.
- (58) Luo, R.; Gilson, M. K. *J. Am. Chem. Soc.* **2000**, *122*, 2934–2937.
- (59) Yu, Y. B.; Privalov, P. L.; Hodges, R. S. *Biophys. J.* **2001**, *81*, 1632–1642.
- (60) Zhu, X.; Yethiraj, A.; Cui, Q. *J. Chem. Theory Comput.* **2007**, *3*, 1538–1549.
- (61) Vallet, V.; Moll, H.; Wahlgren, U.; Szabó, Z.; Grenthe, I. *Inorg. Chem.* **2003**, *42*, 1982–1993.
- (62) Paton, R. S.; Goodman, J. M. *J. Chem. Inf. Model.* **2009**, *49*, 944–955.
- (63) Sponer, J.; Riley, K.; Hobza, P. *Phys. Chem. Chem. Phys.* **2008**, *10*, 2595–2610.
- (64) Sponer, J.; Leszczyński, J.; Hobza, P. *J. Phys. Chem.* **1996**, *100*, 5590–5596.